Momentum balance in a fully developed boundary layer over a staggered array of NREL 5MW rotors

2017 J. Phys.: Conf. Ser. 854 012009

(http://iopscience.iop.org/1742-6596/854/1/012009)

IOP Conf. Series: Journal of Physics: Conf. Series **854** (2017) 012009 doi:10.1088/1742-6596/854/1/012009

Momentum balance in a fully developed boundary layer over a staggered array of NREL 5MW rotors

PL Delafin, T Nishino

Centre for Offshore Renewable Energy Engineering, Cranfield University, Cranfield, MK43 0AL, UK

E-mail: pierreluc.delafin@gmail.com

Abstract. 3D Reynolds-averaged Navier-Stokes (RANS) simulations of a fully developed wind farm boundary layer over a staggered array of NREL 5MW turbines are presented. The turbine is modeled as an actuator disk and as a fully resolved rotor to compare the effect of the turbine model on the wind farm aerodynamics, in particular the streamwise momentum balance across the farm. Results show that the difference in the turbine model affects the average wind speed through the farm as well as the local flow pattern around each turbine; both contributing to the difference in the prediction of farm performance. Results are also compared with a simple theoretical model of very large wind farms proposed recently. The actuator disk simulations agree very well with the theoretical model, whereas the fully resolved rotor simulations show some consistent and expected differences from the model.

1. Introduction

As wind energy is gaining more and more interest for its ability to produce clean, affordable and reliable electricity [1, 2], modeling and simulations of large wind farms are becoming an important subject [3, 4, 5], especially for offshore applications. Actuator disk models are often used in such large wind farm modeling and simulations [3, 5, 6]. There are many earlier studies comparing actuator disk simulations and blade-resolved rotor simulations, but these studies are either for an isolated turbine [7, 8] or a very small number (usually two) of turbines [9, 10], not for large wind farms. Therefore in this study we perform actuator disk (AD) and fully resolved rotor (FRR) simulations of an NREL 5MW horizontal-axis wind turbine in an infinitely large wind farm. The main objective is to analyze how the difference between the AD and FRR simulations will affect the momentum balance across the farm and thus the prediction of farm performance. The results of these simulations will be analyzed in association with the theoretical model of very large wind farms proposed recently by Nishino [5].

2. Theoretical model

The theoretical model proposed by Nishino [5] is a simple quasi-one-dimensional model to predict a practical upper limit to the efficiency of a very large wind farm. The basic concept underlying the Nishino model is similar to the so-called 'top-down' models [11, 12]. However, the Nishino model is based on a simplified 'two-scale coupled' momentum conservation argument and does not consider the details of wind profile across the farm boundary layer explicitly. On one hand, the 'farm-scale' wind speed reduction factor, $\beta = U_F/U_{F0}$ (where U_F is the wind speed averaged

over a nominal farm layer height, H_F, and U_{F0} is its undisturbed equivalent), is calculated from the momentum balance between the driving force of the atmospheric boundary layer and the resistance due to the turbines' thrust and bottom friction. On the other hand, the 'turbine-scale' wind speed reduction factor, $\alpha = U_T/U_F$ (with U_T the face-averaged wind speed over the turbine rotor swept area), is calculated from the classical actuator disk theory. These two wind speed reduction factors α and β satisfy the (simplified) momentum conservation equation [5]:

$$1 - \beta^\gamma = \lambda \cdot \frac{1}{C_{f0}} \cdot \beta^2 \cdot 4\alpha(1-\alpha) \tag{1}$$

where $\lambda = A/S$ is the ratio of the turbine swept area A to the land area S (i.e. farm density) and $C_{f0} = \tau_{w0}/0.5\rho U_{F0}^2$ is the natural bottom friction coefficient.

The only empirical parameter employed in the Nishino model is γ in Eq. 1. This parameter describes how the bottom friction (shear stress) changes in response to the reduction of the average wind speed through the farm layer. γ is defined such that

$$\frac{<\tau_w>}{\tau_{w0}} = \beta^\gamma = \left(\frac{U_F}{U_{F0}}\right)^\gamma \tag{2}$$

where $<\tau_w>$ is the bottom shear stress averaged across the farm. Further details of the Nishino model can be found in [5] and [6].

3. RANS simulations

3.1. Geometry and mesh

An 'infinitely large' array of NREL 5MW rotors is considered in this paper. The 126m diameter (D) turbine is based on the initial design by NREL [13] and takes into account the modifications suggested by Sandia National Laboratories [14] (i.e. a smoother blade thickness distribution and a smoother root/blade transition compared to the initial design). This turbine concept has been widely used [15, 16, 17]. The tip shape, not included in the reference designs [13, 14], is defined as a simple 'rounded' tip and the hub diameter has been increased to 5.4m in this study (to simplify the generation of the structured mesh). The center of the hub is located 90m above the ground which gives a ground clearance of $0.21D$. The rotational axis is tilted by 5° with respect to the horizontal plane and a precone of 2.5° is used for the blades, as defined in [13].

All farm simulations in this study consider a fully developed boundary layer flow driven by a constant streamwise pressure gradient over an 'infinitely large' wind farm, similarly to [3] and [5]. This 'infinitely large' wind farm is modeled as a doubly periodic array of turbines. Only one turbine is placed in the middle of a relatively small ($6D \times 6D$), but periodic, computational domain (Fig. 1(a)). The height of the computational domain is $8D$ ($\sim$ 1km). The turbine is modeled as an Actuator Disk (AD) or as a Fully Resolved Rotor (FRR). Turbines are arrayed in a staggered configuration which means that the streamwise spacing between two turbines is $12D$ (Fig. 1(a)).

Multi-block structured meshes are created for the AD and FRR simulations. The computational domains have the same dimensions in both cases: $(L_x, L_y, L_z) = (6D, 6D, 8D)$. The AD mesh contains a 126m diameter porous disk whose center is located at $x = y = 0$m (center of the domain) and $z = 90$m. An 'O-grid' mesh topology is used inside and around the disk, as shown in Figure 2(a). 104 nodes are used on the disk edge. The first cell height on the bottom boundary (ground) is 1m. Around the disk, the streamwise node spacing starts from 0.5m and expands with a ratio of 1.15 to reach a maximum spacing of 11m near the inlet and outlet boundaries. The maximum lateral (y) spacing is 13m. In total, the AD mesh contains 8×10^5 cells.

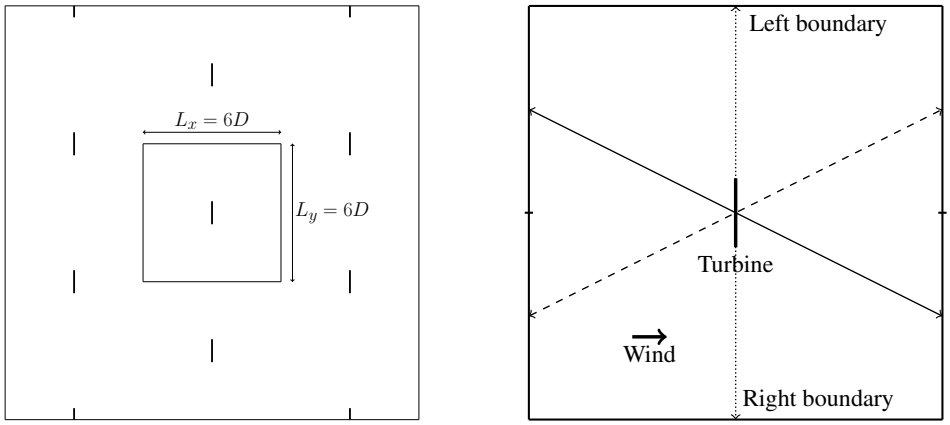

(a) (b)

Figure 1: Horizontal section of the staggered array of rotors (a) and sketch showing the connections (arrows) between the periodic boundaries in a horizontal section of the computational domain (b).

The FRR mesh is divided into two sub-domains: a rotating part containing the three blades and a stationary outer part. The rotor part is meshed with an O-grid topology around the blades. The wall normal spacings ensure $y^+_{max} \sim 1$, except on the hub where wall functions are used to reduce the total number of cells. 186 nodes are used in the chordwise direction and 107 nodes in the spanwise direction for each blade (Fig. 2(b)). This gives 5.7×10^6 cells in the rotor sub-domain. The outer part contains the nacelle and the front part of the hub (i.e. the streamwise extent of the rotor sub-domain is small, Fig. 2(b)). The cell sizes immediately upstream and downstream of the rotor sub-domain are $\Delta x = 0.5$m and 0.1m, respectively, to match the cell sizes with those inside the rotor sub-domain. The maximum streamwise spacing is 6m and the maximum lateral spacing is 7m. The first cell height on the bottom boundary is 1m, as with the AD mesh. The outer sub-domain contains 6.9×10^6 cells. Therefore, the FRR mesh contains 12.6×10^6 cells in total.

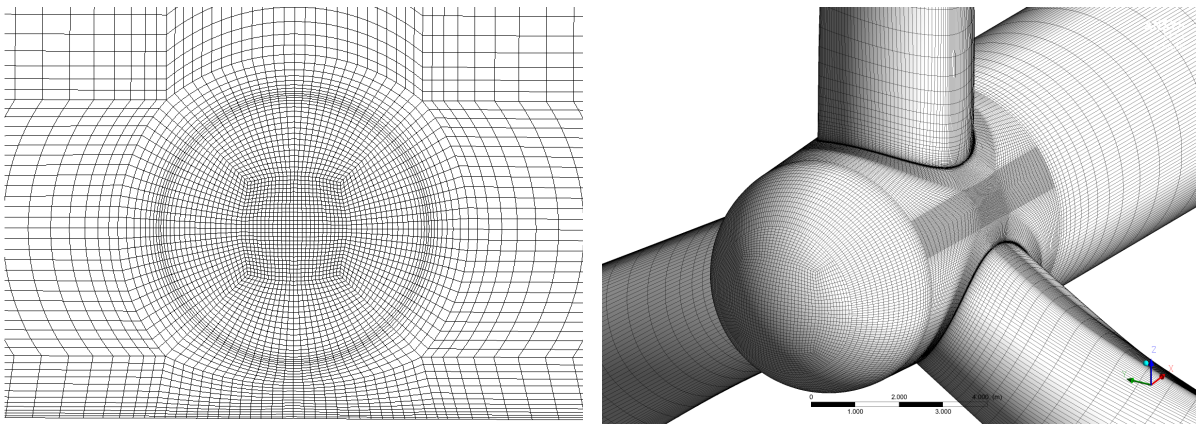

(a) (b)

Figure 2: Computational meshes: (a) cross sectional view around the disk (for AD simulations) and (b) surface mesh of the rotor hub (for FRR simulations).

3.2. Boundary conditions and simulation parameters

In all simulations presented in this paper, the bottom boundary is set as 'wall' with a nominal roughness height $K_s = 1$m or 5m. K_s is a sand-grain type roughness related to the aerodynamic roughness parameter z_0 as $K_s = (E/C)z_0$ [18], where $E = 9.793$ is an empirical constant and $C_s = 0.5$ is the roughness constant. The top boundary is set as 'symmetry'. To model the staggered configuration of the turbines, both inlet and outlet boundaries are vertically split into two equal parts (left and right). Periodic interfaces are then used to connect the right outlet boundary to the left inlet boundary and vice versa (Fig. 1(b)). The side boundaries are set as periodic interfaces. The doubly periodic computational domain obtained enables the simulation of one turbine operating inside an infinitely large wind farm with a staggered configuration. A constant pressure gradient is employed in the streamwise direction for all simulations using the same ground roughness. In the AD simulations, a 'porous jump' condition is used for the disk surface, where a disk resistance K is used to calculate the streamwise momentum sink following the equation $M_x = K(\frac{1}{2}\rho U_d^2)$, where U_d is the local streamwise velocity through the disk [19]. In the FRR simulations, blades are considered as 'wall'.

The Reynolds-averaged Navier-Stokes (RANS) equations are solved using the ANSYS Fluent software [20] with the $k-\omega$ SST turbulence model [21]. In the AD simulations (steady RANS), the SIMPLE algorithm is used for pressure-velocity coupling and second order schemes are used for pressure, momentum and turbulence spatial discretization. In the FRR simulations (unsteady RANS), the pressure-based coupled algorithm is used as it was found to be more stable. Only first order schemes are used for the first rotor revolution; then, 'Standard' scheme is used for the pressure equation and second order schemes are used for momentum and turbulence spatial discretization as well as for the transient formulation. The time step size always corresponds to a variation of the rotor azimuthal angle $\Delta\theta = 0.5^\circ$ and 15 iterations are used per time step. For all simulations, the density and viscosity of air are assumed to be $\rho = 1.225\text{kg/m}^3$ and $\mu = 1.7894 \times 10^{-5}\text{kg/(ms)}$, respectively.

The FRR simulations require to specify an appropriate rotational speed of the rotor. This is not a straightforward task considering that the flow in the fully developed farm boundary layer is not known a priori. Therefore, we use the results of the AD simulations to estimate the wind speed at hub height and $3D$ upstream the turbine. This value ($U_\infty = 6$m/s with $K_s = 1$m and $U_\infty = 6.9$m/s with $K_s = 5$m) is used to calculate the rotational speed of the rotor that corresponds to the tip-speed-ratio (TSR) used in [13] (7.98rpm or TSR = 8.8 with $K_s = 1$m and 8.41rpm or TSR = 8.0 with $K_s = 5$m).

3.3. Single turbine simulation (for validation)

The NREL 5MW turbine has no experimental data available (concept design only). However, [13] gives performance predictions for an isolated turbine with a uniform upstream wind speed, using the FAST code. These data are used for validation of our resolved rotor model before using it for wind farm simulations. One additional mesh for the FRR simulation has been created based on the one described in section 3.1, with extended horizontal dimensions: $(L_x, L_y) = (40D, 40D)$. Unlike the farm simulations with periodic boundary conditions, the bottom boundary is set as 'symmetry' to simulate a uniform (not sheared) flow around the isolated turbine. A uniform wind speed $U_\infty = 11.4$m/s is defined on the upstream boundary with a turbulence intensity of 5% and a turbulent viscosity ratio of 10. The turbulence intensity decays while traveling downstream (as there is no shear) and reaches low values around the turbine ($\sim 0.03\%$). The rotational speed is 12.1rpm which corresponds to TSR = 7.0 [13]. The simulation has been run for 8 revolutions so that the difference of power coefficient between the last two revolutions is sufficiently small (0.77%).

Averaged results of power and thrust coefficients are presented in Table 1. The FRR simulation predicts a C_P value close to the reference value. The predicted C_P is supposed

to be slightly higher than what would be obtained for a perfectly isolated turbine because of the local (partial) blockage effect due to the proximity of the bottom boundary [22]. It should also be noted that the result of the FRR simulation is not supposed to be exactly the same as the reference value since the reference value and the FRR simulation are based on two different numerical methods (BEM and CFD, respectively). However, the fact that the FRR simulation result is close to the reference value suggests that the rotor simulation (in particular the generation of rotor geometry) has been conducted appropriately.

3.4. Empty box simulations

Empty box simulations are run with the AD mesh described in section 3.1. The disk boundary condition is set as 'interior' instead of 'porous jump' and all other boundary conditions are the same as in section 3.2. Simulations are run with both $K_s = 1$m and $K_s = 5$m with a constant mass flow rate. The mass flow rate is calculated based on a power-law velocity profile (with an exponent of 0.1) with a reference wind speed $U_{ref} = 15$m/s at $z = 90$m (hub height). This gives a mass flow rate equal to 16.528×10^6kg/m^3. The empty box simulations are initialized with a uniform velocity field and they are run for about 10^6 iterations to obtain a fully converged flow field. Figure 3 shows the velocity profiles obtained with the two roughness heights. The wind speed is lower with $K_s = 5$m than with $K_s = 1$m in the region of the turbine. The empty box simulation is used to obtain the background pressure gradient (for a given K_s) that will be used in the AD and FRR farm simulations (Table 2). It is also used to obtain some parameters used in the theoretical farm model [5] such as the natural farm-layer wind speed (U_{F0}), the farm layer height (H_F) and the natural bottom shear stress (τ_{w0}). The farm layer height was found to be $H_F = 1.80D$ with $K_s = 1$m and $H_F = 1.76D$ with $K_s = 5$m.

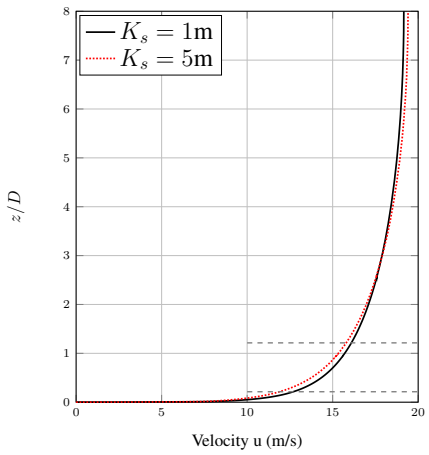

Figure 3: Streamwise velocity profiles of the non-disturbed atmospheric boundary layer with $K_s = 1$m and $K_s = 5$m. The rotor position is represented by the dashed gray lines.

Table 1: Power (P), power coefficient (C_P) and thrust coefficient (C_T) for an isolated turbine with $U_\infty = 11.4$m/s.

	P (MW)	C_P	C_T
FRR	5.60	0.49	0.75
FAST, [13]	5.29	0.47	0.81

Table 2: Summary of pressure gradients obtained from the 'empty box' simulations.

Roughness height, K_s (m)	Pressure gradient (Pa/m)
1	-7.49×10^{-4}
5	-10.59×10^{-4}

3.5. Wind farm simulations

Once the 'empty box' simulations detailed in section 3.4 have been conducted, it is possible to run the farm simulations using the background pressure gradients given in Table 2. The actuator disk simulations have been run for 10^6 iterations to obtain fully converged results (maximum residual = 10^{-11}). The fully resolved rotor simulations use the flow calculated in their corresponding AD simulation (with $K = 2$) as the initial flow condition (except for the

rotor sub-domain). FRR simulations have been run for 92 revolutions ($K_s = 1$m) and 50 revolutions ($K_s = 5$m). After 92 revolutions with $K_s = 1$m, the turbine wake has traveled $26D$ downstream the turbine (assuming the average wind speed calculated between two rotors, along the horizontal line at hub height and going through the nacelle). This means that the wake created at the beginning of the simulation had time to reach the rotor twice (because of the periodic boundary conditions).

Figure 4 shows the variations of (spatially averaged) bottom shear stress with the number of revolutions for both ground roughness heights. The bottom shear seems to follow the same pattern in both cases and is fluctuating close to the value obtained in the AD simulations. The case $K_s = 5$m has been run for only 50 revolutions but the pattern observed for the $K_s = 1$m case suggests that the bottom shear would not vary significantly with additional revolutions.

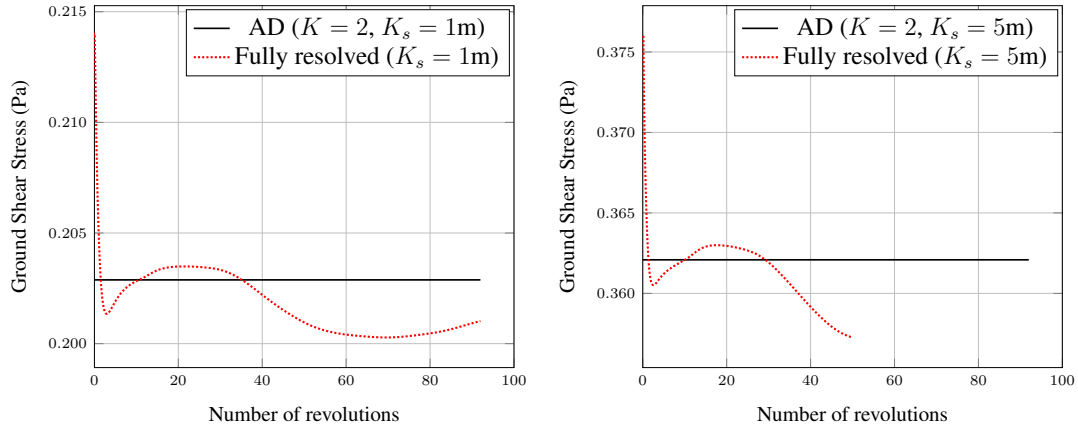

(a) (b)

Figure 4: Average ground shear stress variations with the number of revolutions: (a) $K_s = 1$m and (b) $K_s = 5$m.

Figure 5 shows a comparison of the streamwise velocity profiles obtained from the AD ($K = 2$) and FRR simulations with $K_s = 1$m. The profiles are plotted $1.5D$, $6D$ and $10.5D$ downstream the turbine. At $x/D = 1.5$, the difference between the AD and FRR simulations is significant in

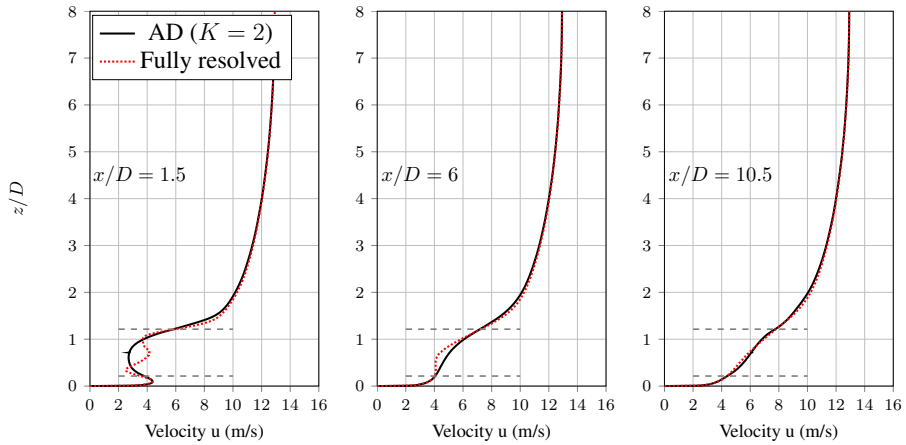

Figure 5: Velocity profiles at different locations in the wake of the rotor, $K_s = 1$m. The rotor position is represented by the dashed gray lines.

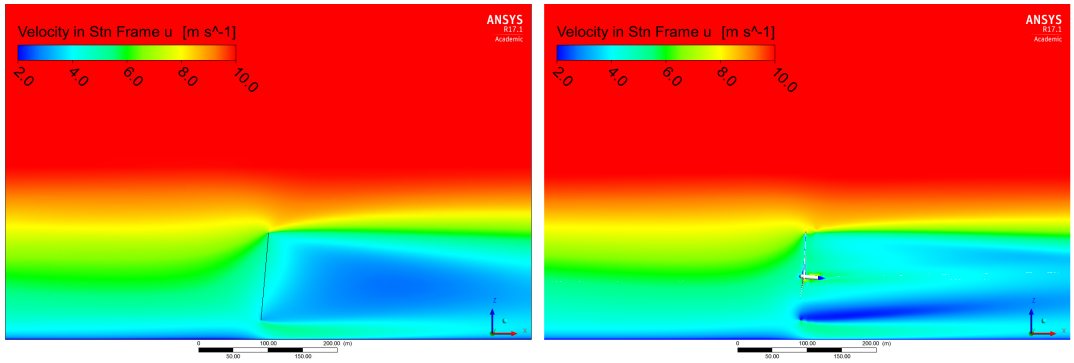

(a)

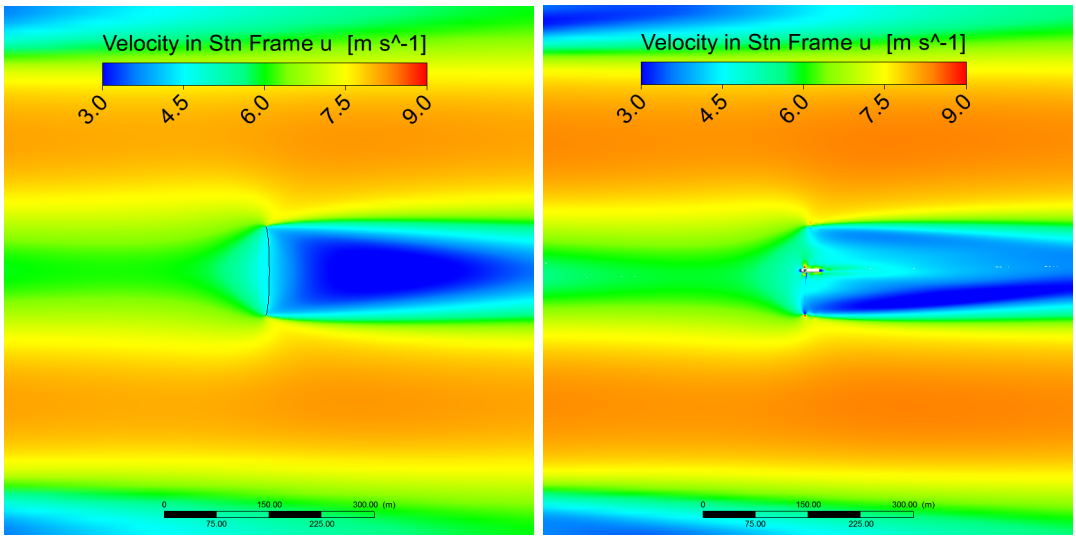

(b)

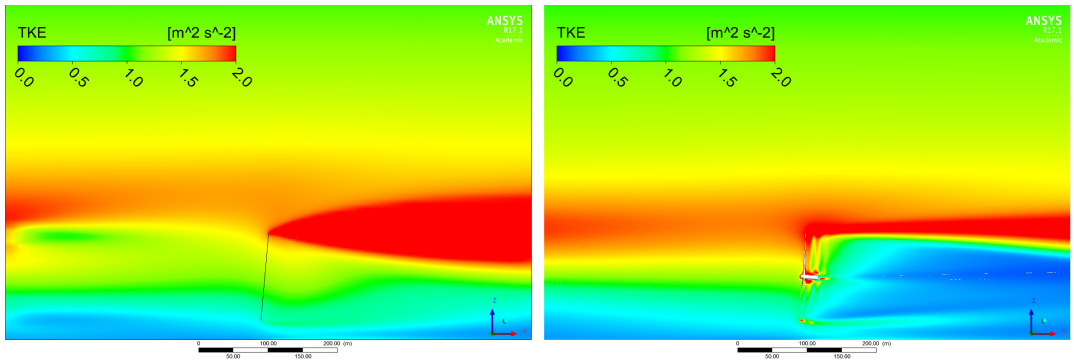

(c)

Figure 6: Flow field comparison between the AD simulation ($K = 2$, left) and the FRR simulation (right) in terms of (a): streamwise velocity in a vertical plane containing the rotor axis, (b): streamwise velocity in a horizontal plane located at hub height and (c): turbulent kinetic energy in a vertical plane containing the rotor axis. $K_s = 1$m.

the rotor area. This has already been observed in previous studies such as [8]. Away from the rotor area, both AD and FRR simulations give very similar results. When x/D increases, the

difference between the AD and FRR simulations decreases. Although not shown in this paper, similar comments can be made for the results obtained with $K_s = 5$m.

Figure 6 shows a comparison of the flow field between the AD ($K = 2$, left) and FRR (right) simulations. Figures 6(a) and 6(b) show the streamwise velocity field in a vertical plane containing the rotational axis and in a horizontal plane at hub height, respectively. In the AD simulation, the wake downstream the turbine is relatively homogeneous, whereas in the FRR simulation, the velocity deficit is more significant in the lower part (Fig. 6(a)) and in the left part of the wake (Fig. 6(b)), when viewed from downwind). However, upstream the turbine and away from the rotor region, both simulations give similar velocity fields. Figure 6(c) shows the turbulent kinetic energy (TKE) field in the vertical plane containing the rotational axis. The TKE values are lower in the wake of the turbine in the FRR simulation compared to the AD simulation. Furthermore, in the FRR simulation, a thin layer of high TKE values can be observed at the top of the wake region, whereas this layer is much wider in the AD simulation. In the upstream region, the vertical distribution of TKE is also affected by the turbine model.

The results of all six wind farm simulations performed in this study are summarized in Table 3, including two additional AD simulations with $K = 1.6$ and 1.2 (for $K_s = 1$m). It should be noted that the results of FRR simulation for $K_s = 5$m are presented in brackets as this simulation may not have converged sufficiently. The coefficients of thrust ($C_T = T/(0.5\rho U_{F0}^2 A)$) and power ($C_P = P/(0.5\rho U_{F0}^3 A)$) are calculated using the undisturbed farm layer wind speed U_{F0}. The 'local' or 'effective' coefficients of thrust (C_T^*) and power (C_P^*) are also calculated using the farm layer wind speed U_F instead of U_{F0}. Similarly to [6], an increase in K_s (or decrease in λ/C_{f0}) results in an increase in C_P and C_T, regardless of the turbine model used. Of particular interest is the comparison between AD and FRR simulations for $K_s = 1$m. It can be seen that the AD simulation with $K = 1.2$ gives a higher C_T but also a lower C_T^* compared with the FRR simulation. This means that it is not possible to match both C_T and C_T^* at the same time between the AD and FRR simulations by adjusting the disk resistance K in the AD simulation. This is essentially because the present AD simulation tends to predict stronger wake mixing and hence a higher β value (i.e. faster average wind speed through the farm layer) than the FRR simulation for a given thrust.

Although the difference in the turbine model affects the average wind speed through the farm as well as the local flow pattern around the turbine, the γ value (defined in Eq. 2) is found to be around 1.9 to 2 in this study regardless of the turbine model used, while this value is around 1.5 to 1.6 in AD simulations in [6]. [6] uses a different turbine diameter ($D = 100$m) and turbine hub height (100m) which may explain the difference in γ observed. It can also be noted that $\gamma = 2.03$ is obtained with the FRR simulation at $K_s = 5$m while this parameter is expected to be smaller than 2 as the turbines usually increase the turbulence intensity within the farm layer [5]. However, as shown earlier in Fig. 6(c), the FRR simulations performed in this study predicted a large low TKE region behind the turbine, which may explain why the value of γ slightly exceeded 2 in this particular case. Note, however, that this may also be due to the RANS simulations not being able to predict the complex near-wake mixing accurately. To confirm this, we would need higher-fidelity simulations, such as detached-eddy simulations, resolving turbulent eddies in the turbine wake.

Figure 7 shows a comparison between the farm simulations and the Nishino model [5] for the power coefficient. As can be seen from the figure and similarly to [6], the agreement between the AD simulations and the theoretical model is very good. The FRR simulations show some consistent discrepancies from the theoretical model. However, the FRR results follow the same pattern as the theory, i.e. C_P increases as λ/C_{f0} decreases. The discrepancies between the theoretical farm model and FRR farm simulations are understandable since the theoretical model employs the classical actuator disk theory as its local (turbine-scale) flow model [5], i.e. the theoretical model considers 'ideal' turbines to predict an upper limit to the farm performance.

Table 3: Summary of computational results for $K_s = 1$m ($\lambda/C_{f0} = 3.93$, $U_{F0} = 14.9$m/s, $\tau_{\omega 0} = 0.7547$Pa) and $K_s = 5$m ($\lambda/C_{f0} = 2.60$, $U_{F0} = 14.4$m/s, $\tau_{\omega 0} = 1.0671$Pa).

Simulation	K_s	α	β	C_T	C_T^*	C_P	C_P^*	$\tau_\omega/\tau_{\omega 0}$	γ
AD ($K = 2$)	1	0.612	0.498	0.188	0.756	0.058	0.471	0.269	1.88
AD ($K = 1.6$)	1	0.647	0.520	0.183	0.675	0.063	0.444	0.288	1.91
AD ($K = 1.2$)	1	0.689	0.553	0.176	0.575	0.068	0.403	0.317	1.94
FRR	1	-	0.509	0.159	0.614	0.042	0.340	0.266	1.96
AD ($K = 2$)	5	0.620	0.574	0.256	0.778	0.093	0.492	0.339	1.95
FRR	5	-	(0.583)	(0.209)	(0.635)	(0.068)	(0.358)	(0.335)	(2.03)

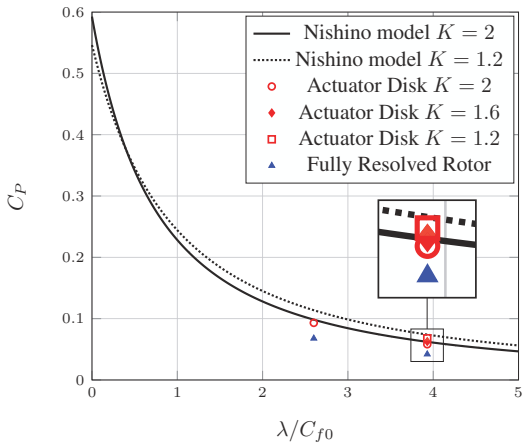

Figure 7: Comparison between the AD and FRR simulations and the Nishino model ($\gamma = 2$).

4. Conclusions

3D RANS simulations of an 'infinitely large' wind farm, consisting of a periodic staggered array of NREL 5MW turbines, have been conducted with two different turbine models: actuator disk and fully resolved rotor. These farm simulations employ an assumption that the atmospheric boundary layer is driven by a constant streamwise pressure gradient, the value of which was obtained (for a given bottom roughness) from the so-called 'empty box' simulation with a fixed mass flow rate. The results show that the difference in the turbine model affects the average wind speed through the farm as well as the local flow pattern around the turbine. In particular, the present actuator disk farm simulations tend to predict stronger wake mixing and hence a faster average wind speed through the farm than the resolved rotor farm simulations. The results have also been compared with the simple theoretical wind farm model proposed recently by Nishino [5]. The actuator disk farm simulation results show a very good agreement with the theoretical model, whereas the resolved rotor farm simulations show some consistent and expected discrepancies from the model. This suggests that the theoretical model could be further extended to predict the performance of real large wind farms in future studies.

5. Acknowledgments

This study was conducted as part of the MULTI-WIND (integrated multi-scale modeling for optimal wind energy extraction) project, supported by EPSRC through the Institutional

Sponsorship Fund allocated to Cranfield University (EP/P511134/1).

References

[1] RenewableUK 2015 Wind energy in the UK, State of the industry report 2015 *Tech Rep*
[2] EWEA 2015 Aiming high, Rewarding ambition in wind energy *Tech Rep*
[3] Calaf M, Meneveau C and Meyers J 2010 Large eddy simulation study of fully developped wind-turbine array boundary layers *Phys. Fluids* **22** 015110
[4] Meneveau C 2012 The top-down model of wind farm boundary layers and its applications *J. Turbul.* **13** N7
[5] Nishino T 2016 Two-scale momentum theory for very large wind farms *J. Phys.: Conf. Ser.* **753** (TORQUE 2016, Munich, Germany) 032054
[6] Zapata A, Nishino T and Delafin PL 2017 Theoretically optimal turbine resistance in very large wind farms *J. Phys.: Conf. Ser.* (Wake Conference 2017, Visby, Sweden) (under review)
[7] Troldborg N, Zahle F, Sorensen NN and Réthoré PE 2012 Comparison of wind turbine wake properties in non-uniform inflow predicted by different rotor models *J. Phys.: Conf. Ser.* **555** (TORQUE 2012, Oldenburg, Germany) 012100
[8] Kalvig S, Manger E and Hjertager B 2012 Comparing different CFD wind turbine modelling approaches with wind tunnel measurements *J. Phys.: Conf. Ser.* **555** (TORQUE 2012, Oldenburg, Germany) 012056
[9] Wilson JM, Davis CJ, Venayagamoorthy SK and Heyliger PR 2015 Comparisons of horizontal-axis wind turbine wake interaction models *J. Sol. Energ. Eng.* **137**
[10] Krogstad PA and Saetran L 2015 Wind turbine wake interactions; Results from blind tests *J. Phys.: Conf. Ser.* **625** (Wake Conference 2015, Visby, Sweden)
[11] Frandsen S 1992 On the wind speed reduction in the center of large clusters of wind turbines *J. Wind Eng. Ind. Aerodyn.* **39** 251-265
[12] Frandsen S, Barthelmie R, Pryor S, Rathmann O, Larsen S, Hjstrup J and Thgersen M 2006 Analytical modelling of wind speed deficit in large offshore wind farms *Wind Energ.* **9** 39-53
[13] Jonkman J, Butterfield S, Musial W and Scott G 2009 Definition of a 5-MW reference wind turbine for offshore system development *Tech Rep* NREL/TP-500-38060
[14] Resor BR 2013 Definition of a 5MW/61.5m wind turbine blade reference model *Tech Rep* SAND2013-2569, Sandia National Laboratories
[15] Bazilevs Y, Hsu AC, Akkerman I, Wright S, Takizawa K, Henicke B, Spielman T and Tezduyar TE 2011 3D simulation of wind turbine rotors at full scale. Part I: Geometry modeling and aerodynamics *Int. J. Numer. Meth. Fluids* **65**
[16] Chow R and van Dam CP 2012 Verification of computational simulations of the NREL 5MW rotor with a focus on inboard flow separation *Wind Energ.* **15**
[17] Tran T, Kim D and Song J 2014 Computational fluid dynamic analysis of a floating offshore wind turbine experiencing platform pitching motion *Energies* **7**
[18] Blocken B, Stathopoulos T and Carmeliet J 2007 CFD simulation of the atmospheric boundary layer: wall function problems *Atmospheric Environment* **41(2)** 238-252
[19] Nishino T and Willden RHJ 2012 Effects of 3-D channel blockage and turbulent wake mixing on the limit of power extraction by tidal turbines *Int. J. Heat Fluid Flow* **37** 123-135
[20] ANSYS Inc. 2016 ANSYS Fluent User's Guide Release 17.1
[21] Menter FR 1994 Two-equation eddy-viscosity turbulence models for engineering applications *AIAA J.* **32**
[22] Nishino T and Draper S 2015 Local blockage effect for wind turbines *J. Phys.: Conf. Ser.* **625** (Wake Conference 2015, Visby, Sweden) 012010